nature communications

Article

https://doi.org/10.1038/s41467-024-54879-7

Bioinspired adaptive lipid-integrated bilayer coating for enhancing dynamic water retention in hydrogel-based flexible sensors

Received: 5 March 2024

Accepted: 21 November 2024

Published online: 04 December 2024

Check for updates

Ming Bai[1], Yanru Chen[1], Liyang Zhu[1,2], Ying Li[3], Tingting Ma[1], Yiran Li[1], Meng Qin[1], Wei Wang[1,4] ✉, Yi Cao[1,2,4] ✉ & Bin Xue[1] ✉

While hydrogel-based flexible sensors find extensive applications in fields such as medicine and robotics, their performance can be hindered by the rapid evaporation of water, leading to diminished sensitivity and mechanical durability. Despite the exploration of some effective solutions, such as introducing organic solvents, electrolytes, and elastomer composites, these approaches still suffer from problems including diminished conductivity, interface misalignment, and insufficient protection under dynamic conditions. Inspired by cell membrane structures, we developed an adaptive lipid-integrated bilayer coating (ALIBC) to enhance water retention in hydrogel-based sensors. Lipid layers and long-chain amphiphilic molecules are used as compact coating and anchoring agents on the hydrogel surface, mimicking the roles of lipids and membrane proteins in cell membranes, while spare lipids from aggregates within hydrogels can migrate to the surface to combat dehydration under deformation. This lipid-integrated bilayer coating prevents the water evaporation of hydrogels at both static and dynamic states without affecting the inherent flexibility, conductivity, and no cytotoxicity. Hydrogel-based sensors with ALIBC exhibited significantly enhanced performance in conditions of body temperature, extensive deformation, and long-term dynamic sensing. This work presents a general approach for precisely controlling the water-retaining capacity of hydrogels and hydrogel-based sensors without compromising their intrinsic physical properties.

Flexible wearable sensors are capable of detecting an extensive range of physical and chemical signals and exhibit adaptability to various forms. This adaptability makes them exceptionally versatile for applications, such as human medicine[1–3], robotics[4], and intelligent materials[5–7]. Broadly, flexible sensors can be categorized into two types: electronic sensors built on elastomers, such as polydimethylsiloxane (PDMS)[8,9], polyurethane (PU)[10], or polyester (PET)[11,12], and ionic sensors[13–15] developed from hydrogels, ionogels, ionic elastomers and so on. Compared with conventional electronic sensors, the ionic conductivity of hydrogels is especially suitable for advanced mechanical, chemical, and electrical sensing of physiologically relevant signals[16,17]. Additionally, they also exhibit biocompatibility[18] and adaptable mechanical compliance[11,19], providing better interfacing with human tissue and organs[13,20].

Despite these advantages, hydrogel-based sensors often suffer from the rapid evaporation of water, which can impact their sensitivity

[1]Collaborative Innovation Center of Advanced Microstructures, National Laboratory of Solid State Microstructure, Department of Physics, Nanjing University, Nanjing, China. [2]Jinan Microecological Biomedicine Shandong Laboratory, Jinan, China. [3]Institute of Advanced Materials and Flexible Electronics (IAMFE), School of Chemistry and Materials Science, Nanjing University of Information Science & Technology, 219 Ningliu road, Nanjing, China. [4]Institute for Brain Sciences, Nanjing University, Nanjing, China. ✉e-mail: wangwei@nju.edu.cn; caoyi@nju.edu.cn; xuebinnju@nju.edu.cn

and mechanical properties. Two primary strategies can address long-term water loss: bulk engineering with water-retaining components or integrating protective layers. For example, replacing water with organic solvents like glycerol, ethylene glycol, and sorbitol can create organic hydrogels with exceptional anti-freezing and non-drying properties[21–23]. However, the use of organic solvents may negatively affect the conductivity of hydrogels, limiting their application in wearable flexible sensors. Protective layers, such as elastomer or composite coatings, have shown significant stretchability and water retention capabilities[24,25]. Nevertheless, internally crosslinked protective layers may impact the flexibility and integrity of the hydrogel under large deformations due to the mismatched mechanical properties and interfacial energies between the water-retaining layer and the hydrogel surface[26–28]. Additionally, tethered supported bilayers, such as lipid membranes, have been raised to provide robust resistance to dehydration and swelling[29–31]. However, the dynamic performance and coating cracks generated[24] during deformations cannot ensure consistent water retention under dynamic loadings, although the physical properties of the bulk materials would not be significantly affected. For example, in a band-shaped hydrogel, the upper surface area (S_O) of the hydrogel under deformations may exceed the original area (S), leading to cracks in the tethered layers and subsequent dehydration of hydrogels (Supplementary Fig. 1). As such, developing water-retention strategies for hydrogel-based flexible sensors remains a challenge, especially considering that flexible hydrogel sensors often experience dynamic deformation (stretching, bending, and twitching), particularly when designed as wearable sensing devices for human joints[14,18,32].

Taking inspiration from dynamic lipid-bilayers of cell membranes, we developed an adaptive lipid-integrated bilayer coating (ALIBC) to generally enhance water retention in various hydrogels. By using self-assembled lipids as the rigid bilayer and long-chain amphiphilic molecules linked to the hydrogel network as anchoring agents, the fluid mosaic structured ALIBC was fabricated successfully. Additionally, standby lipids were stored in the hydrogel matrix as aggregates to fill the cracks of the bilayer coating under deformations through internal-surface migrations. This cell membrane-mimicking coating demonstrates impressive water retention capabilities, retaining 49.3% and 47.3% of water under static conditions and dynamic loading cycles within 48 h, respectively. Furthermore, it preserves the intrinsic flexibility, conductivity, and no cytotoxicity of hydrogels. As a result, the hydrogel-based sensors maintain consistent sensing performance even at body temperatures or under dynamic deformation. Considering the universality of ALIBC on various hydrogel networks, this innovative approach is expected to greatly expand the applications of hydrogel-based flexible sensors in challenging conditions.

Results and Discussion

Design and preparation of an adaptive lipid-integrated bilayer coating (ALIBC)

Previous research has demonstrated that the cell membrane is dynamic by tracking the movements of membrane proteins and lipid molecules, and the stability of the cell surface primarily depends on the interconnection between the cytoskeleton and membrane proteins (left of Fig. 1a)[33]. To fabricate a surface coating similar to fluid mosaic structures of the cell membrane, we incorporated long-chain amphiphilic molecules (undec-10-enoic acid, denoted as UA) into the polymer network onto the hydrogel surface. These molecules serve as anchoring agents for lipids and connect to the hydrogel skeleton (right of Fig. 1a). Amphiphilic lipid molecules assemble on the hydrogel surface and form rigid bilayers together with anchoring agents, which can effectively retain water. The introduction of the UA layer enhances the stability of lipid layers while maintaining their dynamic nature, thereby leading to negligible effects on other physical properties of hydrogels even under deformation. Additionally, spare lipids are stored in hydrogels as aggregates, and these lipids can migrate to the cracks of lipid layers on deformed surfaces, ensuring effective water retention under dynamic conditions (Fig. 1b). By fine-tuning the dynamic characteristics of lipid coating layers, the water retention in hydrogel sensors can be significantly enhanced without affecting their inherent properties.

Specifically, the polyacrylamide (PAAm) hydrogel was used as the model hydrogel matrix, and undec-10-enoic acid (UA), a long-chain hydrophobic molecule with a double bond at one end and a carboxyl group at the other, was used as the long-chain amphiphilic molecule (left of Fig. 1c). UA was linked to the hydrogel network via copolymerization with acrylamide. After the assembly of lipids on hydrogel surfaces, UA would be constrained to bundles and form mosaic patterns with lipids, which are exactly similar to the fluid mosaic structure of the cell membrane.

In the preparation of hydrogels with ALIBC, a surface-assisted self-assembly technique was specially designed to integrate UA molecules onto the hydrogel surface (Supplementary Fig. 2). By immersing an aluminum plate in hexane solution (containing 1 mM UA), the UA molecules self-assembled on aluminum surfaces due to electrostatic interactions[34]. Using the resulting aluminum sheet as the mold to prepare the PAAm hydrogel, UA can covalently link to the hydrogel surface through copolymerization, ensuring the robust attachment of the UA layer to hydrogel surfaces. Then, the hydrogel was allowed to swell in NaCl solution (1 M) to enhance ion conductivity and generate cracks in the UA layers[32,35]. After being immersed in trichloromethane ($CHCl_3$) containing lipids for 20 s, the cracks were repaired through the filling of lipids driven by hydrophobic interactions, thus forming the lipid-integrated bilayer. Note that the lipid aggregates were inserted in hydrogels in advanced by adding lipids directly to the hydrogel precursor solution[36]. Moreover, two types of lipids with distinct dynamic activities, hydrogenated soy phosphatidylcholine (HSPC) and dimyristoylphosphatidylcholine (DMPC), were used to tune the dynamic properties of lipid layers[36], which can further assess the impact of lipid dynamics on water-retention performance based on ALIBC (right of Fig. 1c). We chose DMPC and HSPC for ALIBC because their gel-to-liquid transition temperatures are around room temperature, which is critical to their dynamics. While long-chain lipids may have a better water retention effect due to the higher rigidity of the bilayer coating, they are typically less soluble in water, which greatly impacts gel preparation. Additionally, longer-chain lipids exhibit poorer dynamics, making it challenging for them to effectively retain water under dynamic conditions.

Fluid mosaic structure and lipid migration in ALIBC

The UA grafting on the hydrogel surface was first confirmed. The ^{1}H-NMR spectra showed signals at 5.78 and 2.34 ppm, indicating the copolymerization of UA and acrylamide (AM), although the ratio of UA in the copolymers was slightly lower than that in the monomer feed (Supplementary Fig. 3a). The peaks at 1637 cm^{-1} in the FT-IR spectra suggested the presence of UA on the hydrogel surface (Supplementary Fig. 3b). Besides, the fluorescence of FITC-labeled UA (UA labeled by fluorescein isothiocyanate) on the hydrogel surface did not recover after quenching as indicated by the evaluation of fluorescence recovery after photobleaching (FRAP), further confirming the stable linking between UA and the hydrogel network (Supplementary Fig. 4). It is worth mentioning that UA was only found on the surface of the hydrogels, suggesting that UA was grafted to the hydrogel surface during polymerization rather than dispersing into the interior of the hydrogel (Supplementary Fig. 5). Moreover, for non-covalent crosslinked hydrogels, we anticipate that amphiphilic block polymers could play similar stabilizing roles as UA in covalently crosslinked hydrogels, based on existing literature[37]. We plan to investigate this thoroughly in future studies.

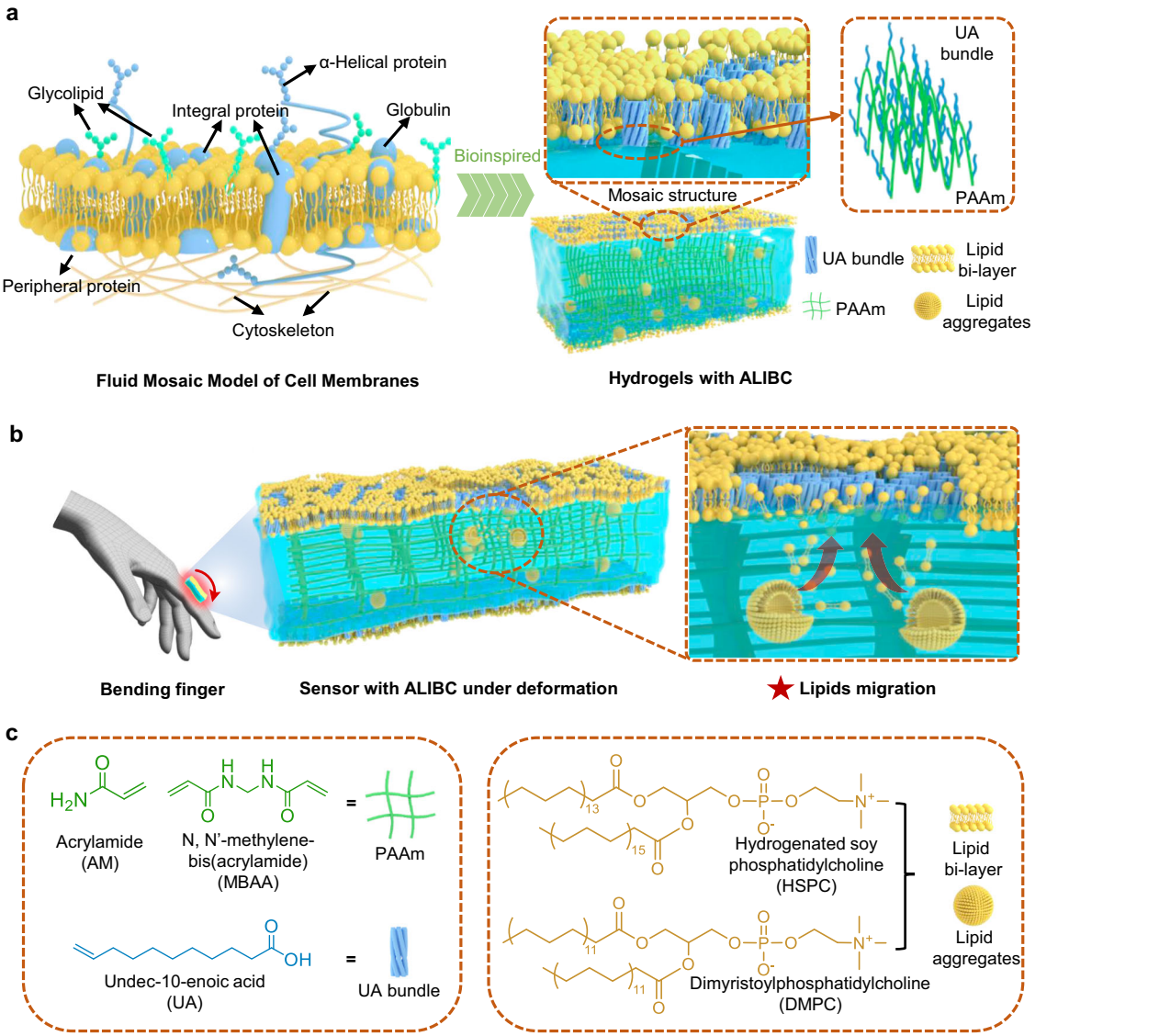

Fig. 1 | Engineering of the adaptive lipid-integrated bilayer coating (ALIBC) and water retention of hydrogel sensors based on ALIBC. a Schematic illustration of the adaptive lipid-integrated bilayer coating (ALIBC) for hydrogel and internal lipid aggregates. **b** Schematic illustration of the dynamic migration of lipids from internal aggregates to cracks of ALIBC under deformation of hydrogels. **c** Chemical structures of monomers (green) forming PAAm gels, UA (blue) forming surface hydrophobic bundles and lipids (yellow) forming the lipid bi-layer and aggregates.

Then, HSPC was used as the lipid to fabricate ALIBC. The UA/lipid-coated PAAm hydrogel (denoted as PAAm-UA/lipid hydrogel) was semitransparent, indicating the presence of a lipid coating and aggregates (Supplementary Fig. 6). Conversely, UA-coated PAAm (denoted as PAAm-UA hydrogel) and PAAm hydrogel remained transparent (Supplementary Fig. 6). Owing to the rigid and hydrophobic coating of UA and lipids, the hydrophilicity of the hydrogel surface after coating was altered. The contact angles of water on the PAAm, PAAm-UA and PAAm-UA/lipid hydrogels were 40.4°, 92.3° and 87.5°, respectively, indicating the transition from a hydrophilic surface to a hydrophobic surface (Supplementary Fig. 7). More importantly, the mosaic structure of ALIBC was investigated by confocal Raman chemical imaging of different hydrogel surfaces (Fig. 2a, b), in which the colors represented the distribution of different components. The color conversion from cyan in the PAAm hydrogel to blue in the PAAm-UA hydrogel indicated that the surface was almost fully covered with grafted UA molecules (Fig. 2b). Moreover, a mosaic-like color distribution of blue (UA) and yellow (lipid) was observed on the surface of the PAAm-UA/lipid hydrogel, suggesting similar structures of ALIBC and cell membranes (Fig. 2b). From the Raman images and equivalent area ratios of UA and lipids on PAAm-UA/lipid hydrogel surfaces, we can also conclude that the spatial distribution of UA and lipids in ALIBC was homogeneous (Fig. 2c). Furthermore, the impact of UA on the fluidity of lipids was investigated using FRAP. The redistribution of lipids in the presence of grafted UA was much slower than in its absence, indicating enhanced stability of the adaptive lipid layers due to the interconnection between UA and hydrogel networks (Fig. 2d, e and Supplementary Fig. 8).

To directly track the dynamic migration of internal and surface lipids, their distributions were monitored using fluorescent labeling-assisted 3D reconstructions based on laser confocal fluorescence microscopy (LCFM). Typically, lipids from inside aggregates and surface coating were stained with DiI (red) and DiO (green) dyes, respectively (Fig. 2f). Owing to the amphiphilic property, the internal lipid molecules can form aggregates in hydrogels (left of Fig. 2f) or lipid coatings on hydrogel surfaces (right of Fig. 2f). Upon stretching, the aggregates may break under the internal stress from the deformed hydrogel network, and the released small lipid fragments would

https://doi.org/10.1038/s41467-024-54879-7

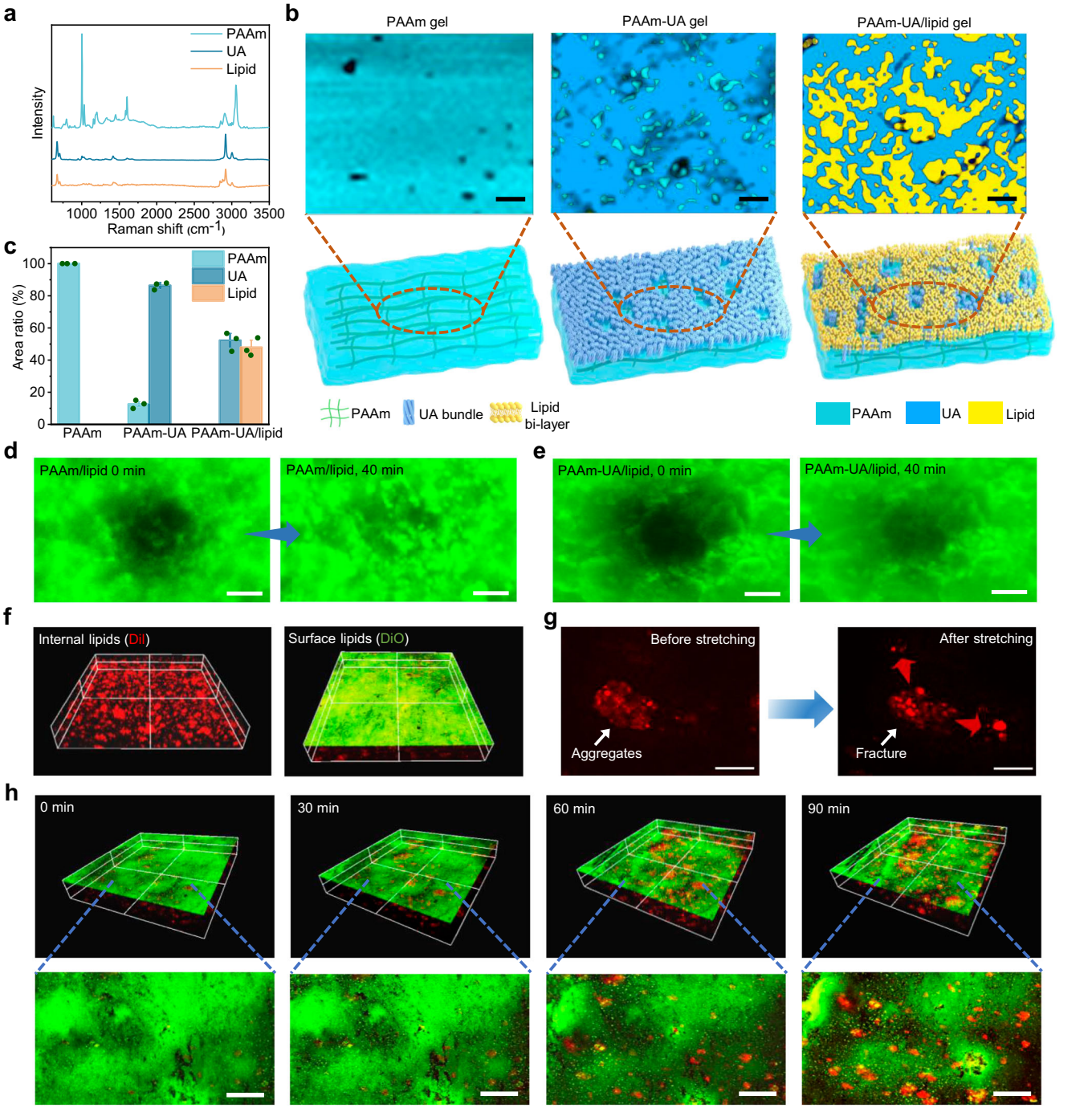

Fig. 2 | Fluid mosaic structures and lipid migration in ALIBC. a Raman spectroscopy of PAAm, UA and lipids (HSPC). **b** Confocal Raman images showing the main components of the surfaces of the PAAm, PAAm-UA and PAAm-UA/lipid hydrogels (scale bar = 20 μm). **c** Area ratios of different components of hydrogel surfaces. Values represent the mean and standard deviation ($n = 3$). **d**, **e** Typical images during a FRAP experiment for fluorescent lipids (DiO-labled HSPC) in hydrogel coating in the absence (**d**) and presence (**e**) of UA (scale bar = 200 μm). **f** 3D reconstruction of hydrogels with internal and surface lipids labeled with DiI (red) and DiO (green) dyes using LCFM. The scanning area was 636.4 μm × 636.4 μm × 200 μm. **g** Fluorescence images (side view) for breakage and outwards migration of internal lipid aggregates in the hydrogel upon stretching (scale bar = 20 μm). **h** Tracking internal and surface lipids in hydrogels under stretching with 3D reconstruction of hydrogels using LCFM. The same area of hydrogel was scanned every 30 min under a constant stretching of 50%. The top channel corresponds to 3D reconstructions, while the bottom channels correspond to the surface of the area. The scanning area was 636.4 μm × 636.4 μm × 200 μm. The scale bar of the bottom channel is 100 μm.

migrate to the hydrogel surfaces to fill the cracks of the surface coating (Fig. 2g). Since the mesh size of the PAAm hydrogel is smaller than 30 nm (Supplementary Fig. 9), significantly smaller than the micro-sized lipid aggregates, we anticipate that the internal lipids would either migrate together with the deformed hydrogel network or traverse through the hydrogel network under the dynamic perturbation caused by the mechanical deformation of polymer networks. This dynamic loading causes the polymer strands to extend, enlarging the mesh size and facilitating the migration of trapped lipid aggregates. Additionally, the deformation mechanically perturbs the interactions between the polymer network and the lipids, promoting their movement.

To study the outward lipid migration, the same location on the surface of PAAm-UA/lipid hydrogels under stretching was scanned every 30 min (Fig. 2h). Red lipids were observed on the stretching hydrogel surface with increasing time, suggesting the migration of lipids from inside aggregates to outside. The cracks generated during stretching were filled with migrated lipids rapidly, as indicated by the area with merged colors (Fig. 2h). The fluorescence intensity and area ratios of migrated lipids (red) from internal aggregates on the surface reached ~23.4% and ~14.6% in 90 min (Supplementary Fig. 10). As shown in Supplementary Fig. 11, red lipids were still observed on the hydrogel surface after returning from the tensile state to the initial state. This indicates that the red lipids were indeed migrated to the surface and stayed on the surface when the hydrogels were not stretching. Such a behavior cannot be explained by assuming that the red lipids were just exposed when the hydrogels were deformed with enlarged surface area. Furthermore, surface lipids (green) were observed inside the hydrogels under stretching, suggesting that the lipids can also migrate inward (Supplementary Fig. 12). In contrast, no significant migration between internal and surface lipids was observed for hydrogels without undergoing stretching, indicating that the active lipid migration can be mainly attributed to the deformation of hydrogels (Supplementary Fig. 13). All these results validated the fluid mosaic structures of ALIBC and the bidirectional migration of lipids.

Water-retention performance of hydrogels with ALIBC

Next, the water-retention performances of hydrogels with ALIBC were evaluated in detail. HSPC and DMPC were used to fabricate ALIBC, and the resulting hydrogels were named PAAm-UA/HSPC and PAAm-UA/DMPC, respectively. The solid contents of different hydrogels remained consistent in the anti-dehydration tests (Supplementary Fig. 14). As indicated by dehydration tests (25 °C and 50% humidity), the PAAm-UA/HSPC hydrogels exhibited significantly enhanced water retention and held a weight ratio (normalized remaining mass) of ~71.3% within 6 h, compared to ~23.7% for the PAAm hydrogel (Fig. 3a, b and Supplementary Fig. 15). The PAAm-UA/DMPC hydrogel showed a moderate enhancement of water retention because of the higher dynamics of DMPC. Compared to hydrogels without UA (PAAm/DMPC and PAAm/HSPC), UA-grafted hydrogels (PAAm-UA/DMPC and PAAm-UA/HSPC) showed an increase of 4.8–21.4% in water retention properties (Fig. 3b). This can be attributed to the UA layer acting as anchoring agents to immobilize the lipid bilayer, thereby restricting the mobility of the lipid coating and preventing water evaporation (Fig. 2d, e and Supplementary Fig. 8). Notably, PAAm-UA hydrogels exhibited similar dehydration behavior to PAAm hydrogels, indicating that a single UA layer alone is not sufficient to significantly enhance the water retention of the hydrogels. The thermal gravimetric analysis (TGA) revealed the presence of free water within the PAAm-UA/HSPC hydrogel even after 48 h of drying, further suggesting the enhanced water-retention performances of hydrogels with ALIBC (Supplementary Fig. 16).

Moreover, ALIBC can also be applied to enhance the water retention performances of polyacrylic acid (PAA) and polyethylene glycol diacrylate (PEGDA) hydrogels, highlighting the versatility of this strategy (Supplementary Fig. 17). Additionally, the introduction of NaCl into the hydrogels, which was necessary for sensor fabrication, did not affect their water retention capability (Supplementary Fig. 18).

To further explore the impact of lipid dynamics on hydrogel water retention, the dehydration of hydrogels with ALIBC formed by mixed DMPC and HSPC at various proportions was also studied (Fig. 3c and Supplementary Table 1). The dynamic activity constant of lipids was defined as ($1\text{-}W_{HSPC}/W_{DMPC}$), in which W_{HSPC}/W_{DMPC} corresponds to the mass ratio of HSPC and DMPC. As shown in Fig. 3c, the weight ratio of hydrogels at 6 h decreased with increasing dynamic activity constants, which can be well fitted to a quadratic function. This strategy enables the tuning of desired water retention properties for specific applications, such as promoting wound healing in a moist environment while avoiding excessive humidity that may exacerbate ulceration.

In practical applications for flexible sensors, the water retention performance of hydrogels under deformation was more important than that in static states. By introducing the lipid aggregates into the hydrogel matrix, the internal lipids may dynamically migrate towards the surface to repair the cracks of the lipid coating, ensuring water retention under deformation. To this end, we evaluated the water-retention performance of hydrogels with different coatings under dynamic loading of 300% strain for 48 h (Fig. 3d, e and Supplementary Fig. 19). Hydrogels containing internal lipids demonstrated dynamic water retention performance after more than 30,000 cycles of stretching-relaxation. PAAm-UA/HSPC hydrogels maintained their integrity after 48 h of cyclic stretching-relaxation, whereas PAAm hydrogels fractured after 3 h due to dehydration (Fig. 3d). Notably, PAAm-UA/HSPC hydrogels retained 50% of their initial weight after 48 h of dynamic loading (Fig. 3e), which was comparable to the weight ratio of unstretched hydrogels (Fig. 3b). Moreover, the water retention performance of PAAm-UA/HSPC hydrogels remained almost unchanged before and after 1000 cycles of stretching-relaxation, indicating that their water retention capability can be maintained even after multiple stretching-relaxation cycles (Supplementary Fig. 20).

Furthermore, the weight ratio of PAAm-UA/HSPC hydrogels containing internal lipids under static loading of 50% strain remained at 46% after 48 h, close to the 50% observed in hydrogels without strain (Supplementary Fig. 21), indicating stable water retention under static deformation. Although PAAm-UA/DMPC hydrogels demonstrated decreased water retention performance due to the higher dynamics of DMPC, they still exhibited enhanced water retention under both dynamic and static loading strains compared to PAAm hydrogels (Fig. 3e and Supplementary Fig. 21). These results validate the excellent water retention performance of hydrogels with ALIBC under both static and dynamic deformation conditions.

Mechanical properties of hydrogels with ALIBC

After verifying the water retention, we then explored the impact of ALIBC on the mechanical properties of hydrogels. Previous studies have indicated that due to the mismatch between the mechanical properties of the coating layers and the hydrogels[14,24,38], the internally crosslinked coating layers may inevitably influence the hydrogel stretchability and modulus (top of Fig. 4a). In contrast, leveraging the adaptiveness of the lipid-bilayer coatings, ALIBC was expected to have a negligible impact on the mechanical properties of hydrogels (bottom of Fig. 4a). As shown by tensile and compressive stress–strain curves, PAAm hydrogels with different lipid coatings exhibited improved fracture strain and strength compared to the control PAAm hydrogel (Fig. 4b, c). Specifically, the PAAm-UA/HSPC hydrogel exhibited the fracture strain of 714.5% and modulus of 83.4 kPa under tension, while the fracture strain and modulus under compression reached 77.1% and 98.4 kPa, slightly surpassing the metrics of the pure PAAm hydrogel (Fig. 4d, e). The tensile and compressive strengths of different hydrogels also exhibited the same trend as their fracture strain and modulus, which can be attributed to the self-assembled lipids acting as dynamic crosslinks to a certain extent (Supplementary Fig. 22). The UA layer did not significantly influence the mechanical properties, as suggested by the similar fracture strains and moduli of hydrogels with and without UA. The elastic moduli of HSPC-coated hydrogels were marginally higher than those of DMPC-coated hydrogels, probably due to the rapid dynamics of DMPC. Moreover, the electrical conductivity and no cytotoxicity of hydrogels were negligibly affected by ALIBC due to the dynamic properties and biocompatibility of lipids (Supplementary Figs. 23, 24). Cell and protein adhesion performance was minimal on hydrogels with ALIBC, suggesting the anti-biofouling capacity which may benefit the applications in physiological conditions such as implantable biosensors or sensing in micro-fluidic bio-

https://doi.org/10.1038/s41467-024-54879-7

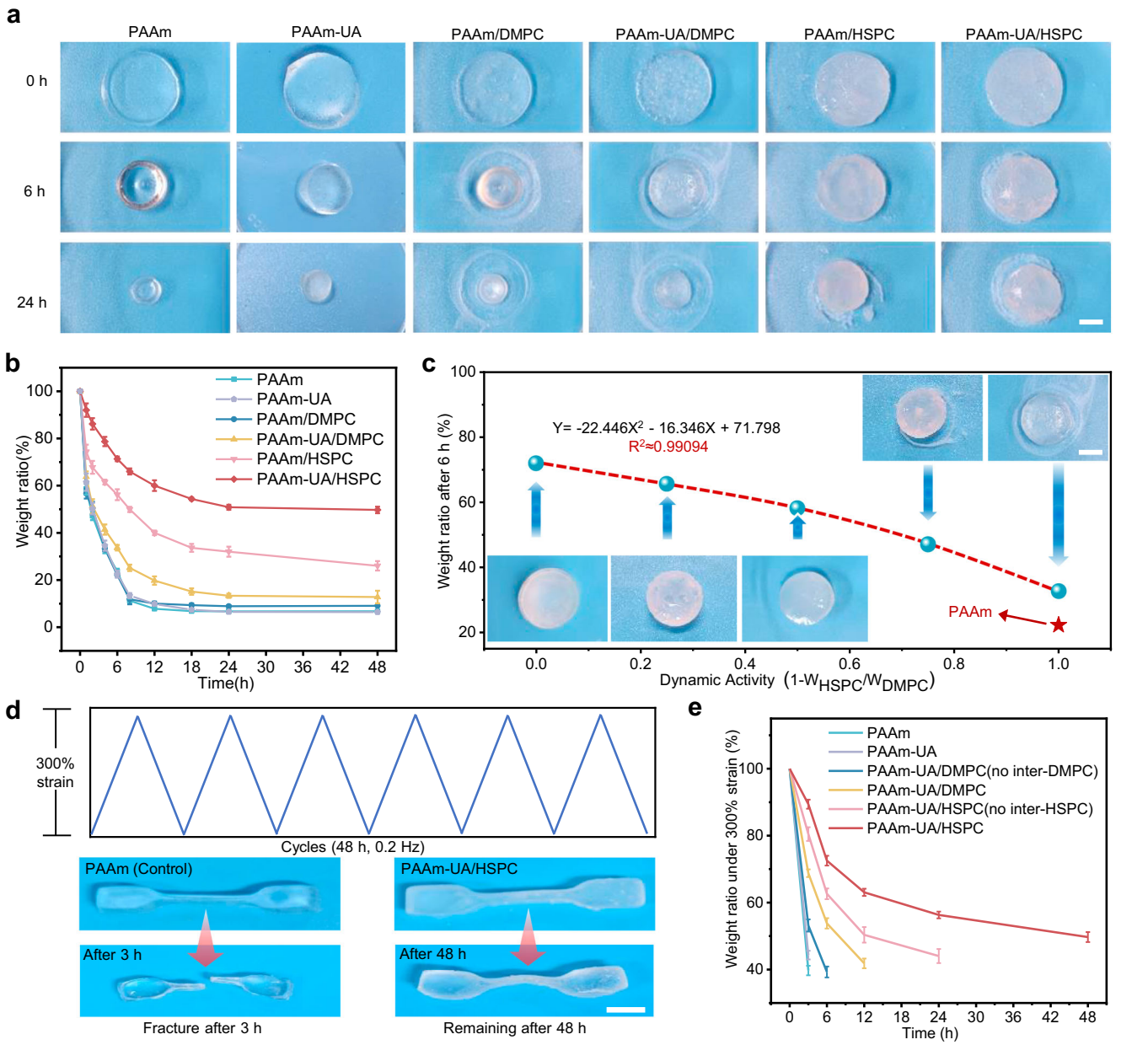

Fig. 3 | Water retention of hydrogels with ALIBC. a Images of hydrogels with different coatings during the dehydration experiments at 25 °C and 50% humidity. Scale bar = 5 mm. **b** Normalized weight ratios (normalized remaining mass) of hydrogels with different coatings within 48 h. **c** Effect of lipid dynamics on the water retention performance of hydrogels within 6 h. Insets correspond to images of hydrogels with coatings of different dynamics after 6 h. Scale bar = 5 mm. **d** Strain signals and images of PAAm (Control) and PAAm-UA/HSPC hydrogels under cyclic stretching-relaxation. PAAm hydrogels fractured after 3 h of cyclic stretching-relaxation while PAAm-UA/HSPC hydrogels maintained their integrity after 48 h. Scale bar = 5 mm. **e** Normalized weight ratios of PAAm (Control), PAAm-UA hydrogels and hydrogels containing ALIBC with and without internal lipid aggregates under cyclic stretching-relaxation (strain ~300%, frequency ~0.2 Hz) for 48 h. Values in (**b** and **e**) represent the mean and standard deviation ($n = 3$).

chips (Supplementary Fig. 25). Besides, the swelling behavior of hydrogels in the presence of salts was negligibly affected by the ALIBC (Supplementary Fig. 26).

Sensing performance of hydrogel-based sensors with ALIBC

Finally, the sensing performance of the hydrogel-based sensor with ALIBC was studied. By enhancing the ion conductivity of PAAm-UA/HSPC hydrogels in preparation using salt ions, a basic resistance sensor for temperature and strain sensing was fabricated (Fig. 5a). The resistance and weight loss of hydrogels with different coatings were monitored under the conditions of 25 °C and 50% humidity for 60 min (Fig. 5b, c). The high correlation of the resistance variation ($\Delta R/R_0$) and weight ratios suggested that the sensing performance of hydrogel sensors was significantly affected by water content. Due to the excellent water retention performance, the resistance variation of the PAAm-UA/HSPC hydrogels remained less than 10%, while that of the PAAm hydrogels reached more than 70%, indicating the potential of improving the long-term sensing performance of hydrogel sensors using ALIBC (Fig. 5b).

Since the resistance of hydrogels can be affected by temperature (Supplementary Fig. 27), the real-time resistance variations of hydrogel sensors with ALIBC under variable temperature cycles were detected to verify the body temperature tolerance (Fig. 5d). The resistance variation of the PAAm-UA/HSPC hydrogel sensors remained stable

https://doi.org/10.1038/s41467-024-54879-7

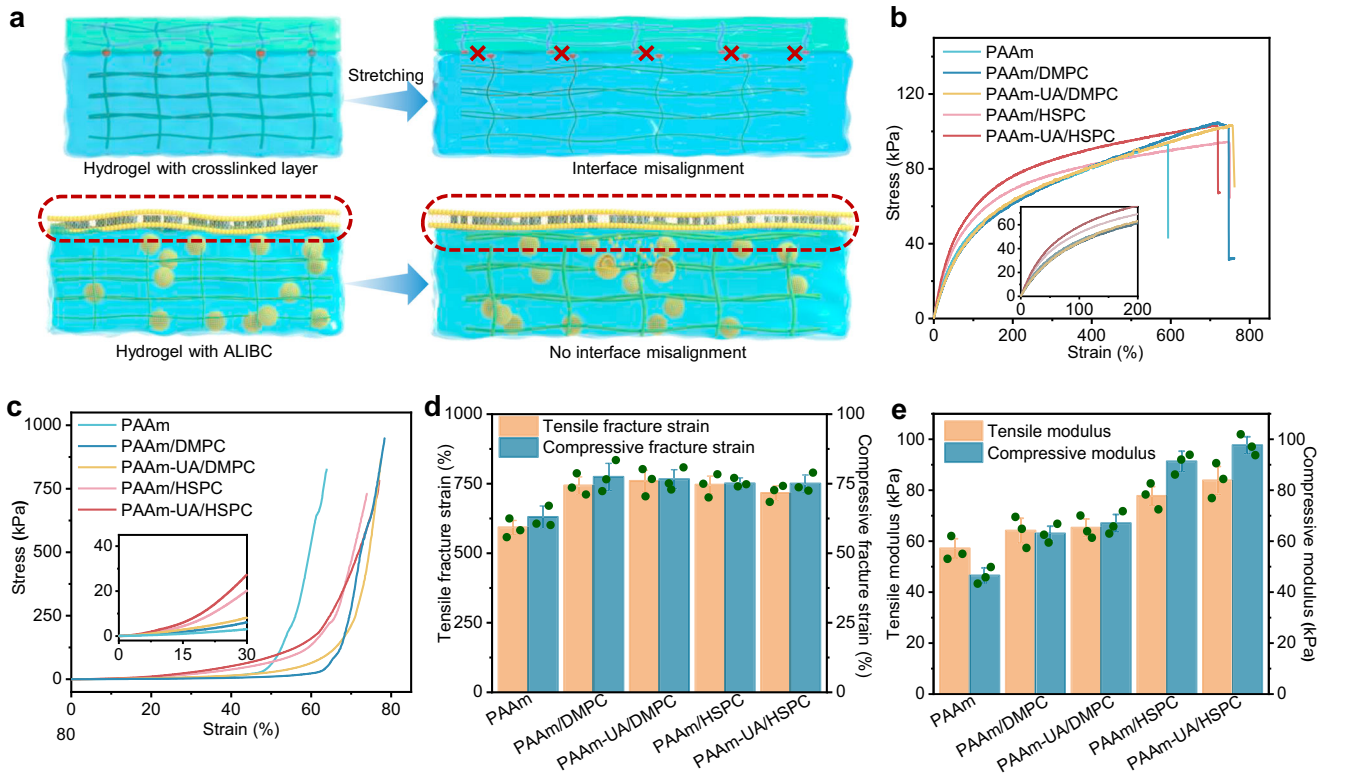

Fig. 4 | Mechanical properties of hydrogels with ALIBC. a Schematic illustration of interfacial misalignment during deformation of different hydrogels. Distinct mechanical responses of the internally crosslinked coating layer and hydrogel matrix during deformation result in interfacial fractures (top channel). In contrast, ALIBC adapts to the deformation of the hydrogel matrix without causing mismatching between coatings and hydrogels (bottom channel). **b**, **c** Typical stress–strain curves of PAAm hydrogels with different coatings under tension (**b**) and compression (**c**). The insets correspond to magnified stress–strain curves at small strains for clarity. **d**, **e**, Fracture strain (**d**) and elastic modulus (**e**) of PAAm hydrogels with different coatings under tension and compression. Values represent the mean and standard deviation ($n = 3$).

under 10 variable temperature cycles with baseline deviations less than 8%. On the other hand, the PAAm hydrogel (control) exhibited significant baseline deviation (~69.7%) after the 10th cycle (Fig. 5d and Supplementary Fig. 28).

Due to the excellent water retention under deformation and body temperature, the hydrogel sensors with ALIBC possessed reliable long-term monitoring of cyclic body motions in air (Fig. 5e). The PAAm-UA/HSPC hydrogel sensors exhibited consistent and distinguishable sensing signals for bending-releasing of finger and elbow in 48 h, with a baseline deviation of less than 8% (Fig. 5f, g). In sharp contrast, the control group of PAAm hydrogels lost flexibility and sensing capability due to a rapid decrease in water content after 6 h. Moreover, the strain sensitivity of the hydrogel sensors was not affected by ALIBC, as revealed by the similar G-factors of the PAAm and PAAm-UA/HSPC hydrogel sensors (Supplementary Fig. 29). Furthermore, we summarized the four strategies of water retention for hydrogels reported to date[21,24,31,39–50] and compared their functionalities with this study (Supplementary Fig. 30).

To demonstrate the advantage of combined water retention and flexibility sensing, we prepared hydrogel-based sensors using reported water-retention strategies (hydrogels with organic solvent, hydrogels with electrolyte, coating-grafted hydrogels, and elastomer-encapsulated hydrogels) and compared their water retention and flexibility sensing performances (Supplementary Fig. 31). All the hydrogels were allowed to reach swelling equilibrium before testing to remove unreacted monomers and enhance conductivity in salt ion solutions. Hydrogels with electrolyte and organic solvent exhibited significantly reduced water retention due to solution exchange during swelling (Supplementary Fig. 31a and c). Elastomer-encapsulated hydrogels also showed decreased water retention due to interfacial mismatching during swelling, leading to exposure of the hydrogels to air (Supplementary Fig. 31b and c). Coating-grafted hydrogels maintained over 80% water retention but exhibited unobservable sensing signals due to poor conductivity (Supplementary Fig. 31d). In contrast, the ALIBC strategy presented in our work demonstrates the optimal combination of sensing and water retention performance (Supplementary Fig. 31e). It can be inferred that the adaptive lipid-integrated bilayer enhanced the water retention of hydrogels without affecting intrinsic properties. Notably, the water retention performance of the hydrogel may decline slightly due to the loss of the lipid bilayer caused by friction with skin or substrates (Supplementary Fig. 32). Despite this, PAAm-UA/HSPC hydrogels still maintain much better water-retaining properties than PAAm hydrogels.

In summary, drawing inspiration from the fluid mosaic model of cell membranes, we have developed a universal water retention strategy for hydrogels without compromising their inherent stretchability, conductivity, and biocompatibility. Our approach entails the incorporation of covalently bonded hydrophobic UA molecules within the hydrogel network, forming an initial water retention layer and serving as an anchor for the subsequent lipid bilayer. The dynamic lipids embedded within long-chain UA form an adaptive lipid-integrated bilayer coating (ALIBC) and further enhance the hydrogel's water retention capacity. Crucially, unlike most traditional water retention methods, the lipid-integrated bilayer is non-internally crosslinked and adaptive, allowing for effective water retention without compromising stretchability, conductivity, and biocompatibility. Our strategy balances water retention while preserving the intrinsic properties of bulk hydrogels, which is often overlooked in traditional

https://doi.org/10.1038/s41467-024-54879-7

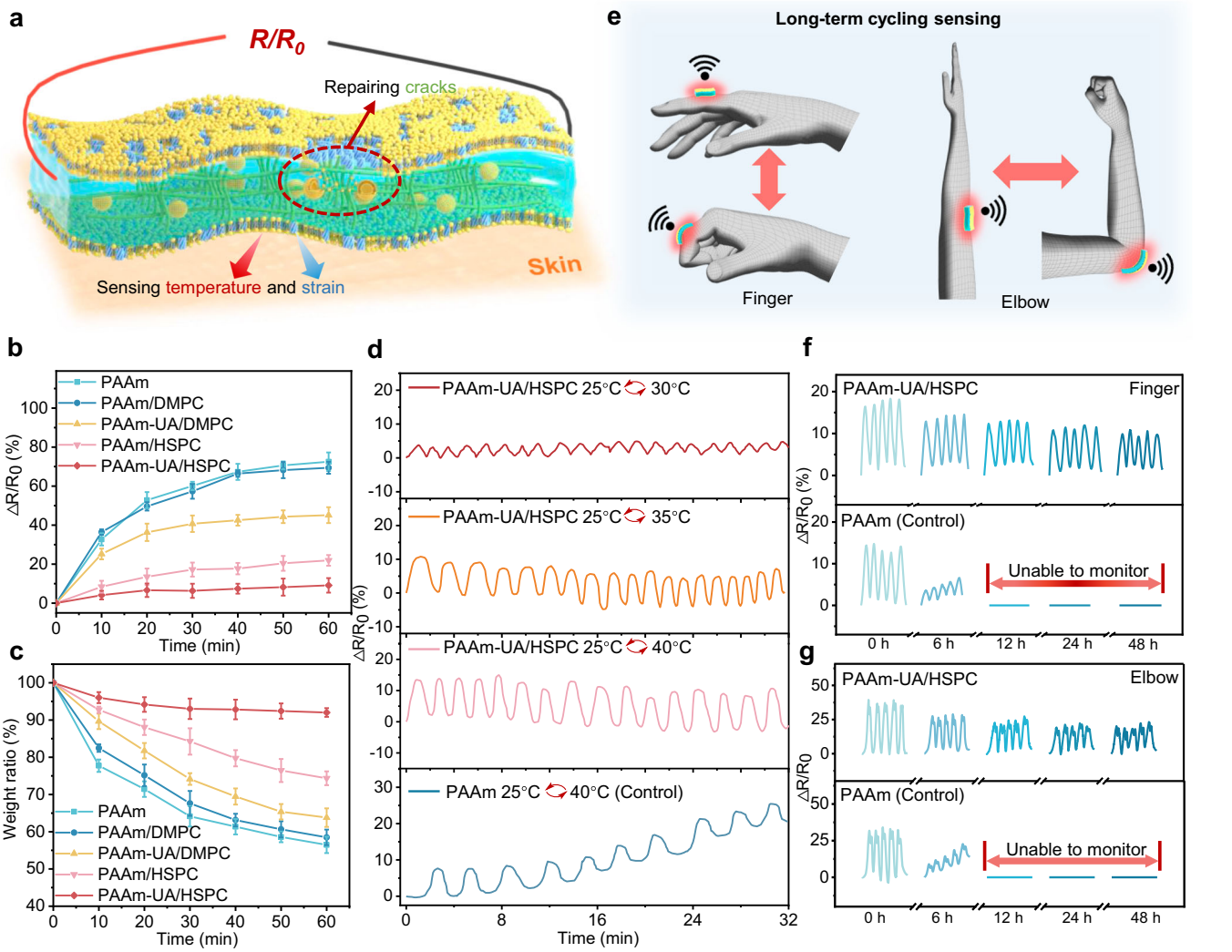

Fig. 5 | Sensing performance of hydrogel-based sensors with ALIBC. **a** Schematic of a hydrogel-based sensor with ALIBC. **b**, **c** Variation of resistances (**b**) and weight ratios (**c**) for hydrogel sensors with different coatings in 1 h. Values represent the mean and standard deviation ($n = 3$). **d** Variation of resistances for the PAAm-UA/HSPC hydrogel sensor under variable temperature cycles. The PAAm hydrogel sensor was used as the control. **e** Schematic of hydrogel-based sensors with ALIBC attached to fingers and elbows for long-term dynamic sensing. **f**, **g** Real-time monitoring for bending-releasing of finger (**f**) and elbow (**g**) using PAAm-UA/HSPC hydrogel sensors in 48 h. The PAAm hydrogel sensor was used as the control.

methods. More importantly, the hydrogel's water retention is reversibly facilitated by the migration of internal lipids to repair cracks, even under prolonged dynamic loading cycles. This ensures the sustained sensing capabilities of the hydrogel-based sensors under dynamic conditions. We firmly believe that this strategy offers a perspective for hydrogel water-retention treatment and significantly expands the application range of hydrogel-based sensors in the field of flexible electronics.

Methods

All the studies of sensing involved human participants were carried out in compliance with the ethical regulations and guidelines of the Ethics Committee of Medical School of Nanjing University (approval number: AP20231123001). Informed written consent from all participants was obtained prior to the research.

Preparation of hydrogels

For the preparation of PAAm-UA/lipid hydrogels, aluminum substrates were immersed in a hexane solution containing UA for 24 h to induce the formation of a dense monolayer of UA on the surface. After evaporation of the solvent, the aluminum sheets were employed as a mold for hydrogel preparation. AM, MBAA, and lipids were dissolved in water/DMSO to concentrations of 3 M, 3 mM and 40 mM, and the resulting solution was subjected to ultrasonication at 60 °C for 2 h. After removing the oxygen with argon, AIBN (3 mM) was added to the solution, and the resulting precursor was transferred into the aluminum mold. After the one-step radical polymerization at 60 °C for 6 h, the hydrogel was immersed in a NaCl aqueous solution for 24 h to achieve swelling equilibrium and ionic conductivity. Eventually, the hydrogel was immersed in $CHCl_3$ solution containing 70 mM lipids to integrate the hydrogel surface with a bilipid layer, thereby achieving hydrogels with ALIBC. HSPC or DMPC were used as the lipids during hydrogel preparation. For the preparation of PAAm-UA hydrogels, UA-coated aluminum sheets were employed as the mold, and the hydrogel was prepared in the absence of lipids as described above. For the preparation of PAAm/lipid hydrogels, aluminum sheets without UA coating were employed as the mold, and the hydrogel was prepared as described above.

Raman spectroscopy and spatial Raman mapping

The Raman spectra were captured with a 10-second integration time spanning the spectral range of 600–3500 cm^{-1} utilizing a Raman system (Horiba JY HR evolution, France) equipped with an Olympus

microscope and a charge-coupled device (CCD) detector. The excitation laser was operated at a wavelength of 532 nm. Calibration was executed using the silicon wafer Raman band at 520.7 cm^{-1}, resulting in a spectral resolution of 0.65 cm^{-1}.

For Raman imaging analysis, the classical least-squares (CLS) model was employed. The averaged Raman spectra of PAAm, UA, and lipid were utilized as basis functions for the CLS analysis. In each pixel, the CLS fitting involved a linear combination of the component spectra (PAAm, UA, and lipid) to optimally match the raw data. Subsequently, false-color images were generated based on the contribution of each component. Data processing and CLS model analysis were conducted using Labspec6 software (Horiba JY).

Fluorescence recovery after photobleaching (FRAP) of lipids

Fluorescence recovery after photobleaching (FRAP) was employed to assess lipid mobility in ALIBC. Hydrogels with lipid (HSPC) coatings in the presence and absence of UA (PAAm-UA/lipid and PAAm-lipid) were used in the experiments. During the preparation of hdyrogels, the hydrogel was immersed in $CHCl_3$ solution containing 70 mM lipids and 30 μM DiO dye for 20 s to endow the lipids on hydrogel surfaces with a lipophilic fluorescence probe (emission wavelength ~569 nm). All hydrogel samples were prepared as disks with a diameter of 1.5 cm and a thickness of 1 mm. The target area on the hydrogel surface was bleached using a 405 nm argon laser at 100% power under a 20× objective lens with a confocal microscope (FV3000-Olympus, Japan). Subsequent imaging was performed under a 10× objective lens. The fluorescence intensity of the central region (500 × 500 μm) was analyzed using Image J (version 1.8.0) to study the fluorescence recovery. FRAP tests were conducted at different locations on the hydrogels, and three samples were used for each group.

Detection of the lipid migration

To enable monitoring the dynamic migration of lipids inside hydrogels, HSPC (5% w.t.) and a lipophilic fluorescence probe (emission wavelength ~569 nm), Dil (0.5% w.t.), were introduced into the precursor solution of the PAAm hydrogel. After taking the hydrogel form molds of aluminum sheets, the hydrogel was immersed in $CHCl_3$ solution containing 70 mM lipids and 30 μM DiO dye (emission wavelength ~501 nm) for 20 s. Then, the band-like hydrogel was held by an adjustable holder and scanned using a laser scanning confocal microscope (FV3000-Olympus, Japan). The fluorescence intensity and area of lipids within both the interior and the surface of the hydrogels with ALIBC were analyzed using Image J (Version 1.8.0).

Anti-dehydration tests for PAAm hydrogels with ALIBC

Hydrogels were prepared as circular disks with a diameter of 1.5 cm and a thickness of 2 mm. The samples were then stored inside a constant temperature and humidity incubator (25 °C and 50% humidity), with their weights recorded. The weight ratio, which was defined as the normalized remaining mass, was used to indicate the water retention performance of the hydrogels. To evaluate the effects of lipid dynamics on the water retention performance, hydrogels with varying dynamic activities of lipids were prepared following the guidelines provided in supplementary Table S1. These hydrogels were subsequently incubated in a constant temperature and humidity incubator (25 °C and 50% humidity). The weights of the samples were recorded and analyzed.

For the evaluation of water retention under deformation, hydrogels with a cross-sectional area of 5 mm^2 and a height of 10 mm were used. Typically, a static loading strain (50%) or dynamic loading strain (300%, 0.2 Hz) was applied to the hydrogel at 25 °C and 50% humidity, during which the weights of the hydrogels were recorded.

Mechanical tests

The mechanical properties were measured with a tensile-compressive tester (Instron 5944 with a 2-kN sensor) at room temperature. Band-shaped hydrogels at a cross-sectional area of 10 mm^2 and a height of 20 mm were used in tensile tests, and the strain rate was kept at 5 mm min^{-1}. Cylindrical-shaped hydrogels with a diameter of 15 mm and a height of 2 mm were used in compressive tests, and the strain rate was kept at 1 mm min^{-1}. Young's modulus for tension and compression comprised the approximate linear fitting values at strains of 0–1 and 0–0.2 mm mm^{-1}, respectively. The toughness was calculated from the area below the stress–strain curve until fracture.

Multifunctional sensing tests

A digital multimeter (Model DMM6500, China), controlled via Kickstrat software, was used to quantify the variations in resistance of the hydrogel with ALIBC under the influence of temperature and stress. $\Delta R/R_O$ is utilized to denote the rate of change in resistance, where R_O signifies the initial resistance and ΔR represents the difference between the initial resistance and the current resistance value. To detect the resistance of hydrogel sensors under variable temperature cycles, the sensors were placed in a thermal cycling chamber (PCTHI-150T, China), and the temperature was switched between two points (25-30 °C, 25-35 °C or 25-40 °C). The temperature was set to switch when the resistance reached a plateau. For the real-time monitoring of finger and elbow motions, a bank-like hydrogel sensor (15 × 25 × 2 mm) was attached to the finger or elbow. Then, the resistances of the sensors in response to bending motions were recorded every 6 h at room temperature.

Reporting summary

Further information on research design is available in the Nature Portfolio Reporting Summary linked to this article.

Data availability

All data are available in the main text or the Supplementary Information. Data is available from the authors on request. Source data are provided with this paper.

References

1. Blache, U. et al. Engineered hydrogels for mechanobiology. *Nat. Rev. Method. Prime.* **2**, 98 (2022).
2. Correa, S. et al. Translational applications of hydrogels. *Chem. Rev.* **121**, 11385–11457 (2021).
3. Cheng, Y. et al. Boosting the piezoelectric sensitivity of amino acid crystals by mechanical annealing for the engineering of fully degradable force sensors. *Adv. Sci.* **10**, 2207269 (2023).
4. Chen, Y. et al. Bioinspired hydrogel actuator for soft robotics: opportunity and challenges. *Nano Today* **49**, 101764 (2023).
5. Wang, J. et al. Semi-convertible hydrogel enabled photoresponsive lubrication. *Matter* **4**, 675–687 (2020).
6. Wang, Z. et al. Stretchable unsymmetrical piezoelectric BaTiO3 composite hydrogel for triboelectric nanogenerators and multimodal sensors. *ACS Nano* **16**, 1661–1670 (2022).
7. Ehrbar, M., Schoenmakers, R., Christen, E. H., Fussenegger, M. & Weber, W. Drug-sensing hydrogels for the inducible release of biopharmaceuticals. *Nat. Mater.* **7**, 800–804 (2008).
8. Varghese, H. et al. A high-performance flexible triboelectric nanogenerator based on cellulose acetate nanofibers and micropatterned PDMS films as mechanical energy harvester and self-powered vibrational sensor. *Nano Energy* **98**, 107339 (2022).
9. Liu, H. et al. An ultrahigh linear sensitive temperature sensor based on PANI: graphene and PDMS hybrid with negative temperature compensation. *ACS Nano* **16**, 21527–21535 (2022).
10. Yang, M. et al. High-performance flexible pressure sensor with a self-healing function for tactile feedback. *Adv. Sci.* **9**, 2200507 (2022).
11. Zhu, L. et al. A rotating paper-based microfluidic sensor array combining Michael acceptors and carbon quantum dots for discrimination of biothiols. *Chem. Eng. J.* **454**, 140065 (2022).

12. Rodriguez, R. D. et al. Ultra-robust flexible electronics by laser-driven polymer-nanomaterials integration. *Adv. Funct. Mater.* **31**, 2008818 (2021).
13. Li, G. et al. Development of conductive hydrogels for fabricating flexible strain sensors. *Small* **18**, 2101518 (2022).
14. Chae, A. et al. Highly oxidation-resistant and self-healable MXene-based hydrogels for wearable strain sensor. *Adv. Funct. Mater.* **33**, 2213382 (2023).
15. Ren, J. et al. An anti-swellable hydrogel strain sensor for underwater motion detection. *Adv. Funct. Mater.* **32**, 2107404 (2022).
16. Li, G. et al. Highly conducting and stretchable double-network hydrogel for soft bioelectronics. *Adv. Mater.* **34**, 2200261 (2022).
17. Liu, X., Zhang, Q. & Gao, G. Solvent-resistant and nonswellable hydrogel conductor toward mechanical perception in diverse liquid media. *ACS Nano* **14**, 13709–13717 (2020).
18. Ru. Fu, X. et al. A stretchable, biocompatible, and self-powered hydrogel multichannel wireless sensor system based on piezoelectric barium titanate nanoparticles for health monitoring. *Nano Energy* **114**, 108617 (2023).
19. Xue, B. et al. Stretchable and self-healable hydrogel artificial skin. *Natl Sci. Rev.* **9**, nwab147 (2021).
20. Pei, X., Zhang, H., Zhou, Y., Zhou, L. & Fu, J. Self-healing and tissue-adhesive Zwitterionic hydrogels as strain sensors for wireless monitoring of organ motions. *Mater. Horiz.* **7**, 1872–1882 (2020).
21. Chen, F. et al. Rational fabrication of anti-freezing, non-drying tough organohydrogels by one-pot solvent displacement. *Angew. Chem. Int. Ed.* **57**, 6568–6571 (2018).
22. Zong, Y. et al. Highly robust and sensitive dual-network freeze-resistant organic hydrogel thermocells. *Carbohydr. Polym.* **314**, 120958 (2023).
23. Chen, H. et al. High toughness multifunctional organic hydrogels for flexible strain and temperature sensor. *J. Mater. Chem. A* **9**, 23243–23255 (2021).
24. Yuk, H., Zhang, T., Parada, G. A., Liu, X. & Zhao, X. Skin-inspired hydrogel-elastomer hybrids with robust interfaces and functional microstructures. *Nat. Commun.* **7**, 12028 (2016).
25. Xu, X., Jerca, V. V. & Hoogenboom, R. Bio-inspired hydrogels as multi-task anti-icing hydrogel coatings. *Chem* **6**, 820–822 (2020).
26. Zheng, Z. et al. Electrodeposited superhydrophilic-superhydrophobic composites for untethered multi-stimuli-responsive soft millirobots. *Adv. Sci.* **10**, 2302409 (2023).
27. Gao, W. & Yu, C. Wearable and implantable devices for healthcare. *Adv. Healthc. Mater.* **10**, 2101548 (2021).
28. Zhu, T. et al. Skin-inspired double-hydrophobic-coating encapsulated hydrogels with enhanced water retention capacity. *Adv. Funct. Mater.* **31**, 2102433 (2021).
29. Lee, B. K., Lee, H. Y., Kim, P., Suh, K. Y. & Kawai, T. Nanoarrays of tethered lipid bilayer rafts on poly(vinyl alcohol) hydrogels. *Lab Chip* **9**, 132–139 (2009).
30. Smith, H. L. et al. Model lipid membranes on a tunable polymer cushion. *Phys. Rev. Lett.* **102**, 228102 (2009).
31. Kibrom, A. et al. Hydrogel-supported protein-tethered bilayer lipid membranes: a new approach toward polymer-supported lipid membranes. *Soft Matter* **7**, 237–246 (2011).
32. Guo, H. et al. Pro-healing zwitterionic skin sensor enables multi-indicator distinction and continuous real-time monitoring. *Adv. Funct. Mater.* **31**, 2106406 (2021).
33. Deisenhofer, J., Epp, O., Miki, K., Huber, R. & Michel, H. Structure of the protein subunits in the photosynthetic reaction centre of rhodopseudomonas viridis at 3Å resolution. *Nature* **318**, 618–624 (1985).
34. Wang, L., Schubert, U. S. & Hoeppener, S. Surface chemical reactions on self-assembled silane based monolayers. *Chem. Soc. Rev.* **50**, 6507–6540 (2021).
35. Cui, W. et al. Strong tough conductive hydrogels via the synergy of ion-induced cross-linking and salting-out. *Adv. Funct. Mater.* **32**, 2204823 (2022).
36. Lin, W. et al. Cartilage-inspired, lipid-based boundary-lubricated hydrogels. *Science* **370**, 335–338 (2020).
37. Kang, J. et al. Enhancing membrane modulus of giant unilamellar lipid vesicles by lateral co-assembly of amphiphilic triblock copolymers. *J. Colloid Interface Sci.* **561**, 318–326 (2020).
38. Pan, S. et al. Mechanically interlocked hydrogel–elastomer hybrids for on-skin electronics. *Adv. Funct. Mater.* **30**, 1909540 (2020).
39. Guo, M. et al. Anti-freezing, conductive and shape memory ionic glycerol-hydrogels with synchronous sensing and actuating properties for soft robotics. *J. Mater. Chem. A* **10**, 16095–16105 (2022).
40. Wu, J. et al. Ultrasensitive and stretchable temperature sensors based on thermally stable and self-healing organohydrogels. *ACS Appl. Mater. Interfaces* **12**, 19069–19079 (2020).
41. Zhao, K. et al. Humidity-tolerant moisture-driven energy generator with mxene aerogel–organohydrogel bilayer. *ACS Nano* **17**, 5472–5485 (2023).
42. Wang, W. et al. Physically cross-linked silk fibroin-based tough hydrogel electrolyte with exceptional water retention and freezing tolerance. *ACS Appl. Mater. Interfaces* **12**, 25353–25362 (2020).
43. Dong, H. et al. Smart polycationic hydrogel dressing for dynamic wound healing. *Small* **18**, 2201620 (2022).
44. Sui, X. et al. Ionic conductive hydrogels with long-lasting anti-freezing, water retention and self-regeneration abilities. *Chem. Eng. J.* **419**, 129478 (2021).
45. Wang, Y. et al. Highly sensitive zwitterionic hydrogel sensor for motion and pulse detection with water retention, adhesive, anti-freezing, and self-healing properties. *ACS Appl. Mater. Interfaces* **14**, 47100–47112 (2022).
46. Gao, W. et al. A Quenched double-hydrophilic coating for the enhancement of water retention of hydrogels. *Adv. Funct. Mater.* **33**, 2303306 (2023).
47. Feng, J. et al. Leeches-inspired hydrogel–elastomer integration materials. *ACS Appl. Mater. Interfaces* **10**, 40238–40245 (2018).
48. Li, H. et al. Asymmetric bilayer CNTs-elastomer/hydrogel composite as soft actuators with sensing performance. *Chem. Eng. J.* **415**, 128988 (2021).
49. Wang, C. et al. Customization of conductive elastomer based on PVA/PEI for stretchable sensors. *Small* **16**, 1904758 (2020).
50. Feng, H. et al. Reversing hydrogel adhesion property via firmly anchoring thin adhesive coatings. *Adv. Funct. Mater.* **32**, 2111278 (2022).

Acknowledgements

This research is supported mainly by the National Natural Science Foundation of China (Grant Nos. T2225016, T2322010 and 11934008), the National Key R&D Program of China (Grant No. 2020YFA0908100 and 2023YFC3605802), the Natural Science Foundation of Jiangsu Province (Grant No. BK20220120), Fundamental Research Funds for the Central Universities (Grant No. 020414380232), and the Shandong Provincial Laboratory Project (Grant No. SYS202202).

Author contributions

B.X., Y.C., W.W., and M.B. conceived the idea and designed the study. M.B. performed the experiments. M.B. and B.X. analyzed the results. Y.C., L.Z., Y.L., T.M., Y-R. L. and M. Q. help design and discussed the experiments. B.X., Y.C. and M.B. wrote and refined the paper. B.X., Y.C., and W.W. supervised the project. All the authors discussed the results.

Competing interests

The authors declare that they have no competing interests.

Additional information

Supplementary information The online version contains supplementary material available at https://doi.org/10.1038/s41467-024-54879-7.

Correspondence and requests for materials should be addressed to Wei Wang, Yi Cao or Bin Xue.

Peer review information *Nature Communications* thanks the anonymous reviewers for their contribution to the peer review of this work. A peer review file is available.